Study of the $pd \rightarrow pd\eta$ reaction

N. J. Upadhyay,[1,*] K. P. Khemchandani,[1,2,†] B. K. Jain,[1,‡] and N. G. Kelkar[3,§]

[1]*Department of Physics, University of Mumbai, Vidyanagari, Mumbai-400 098, India*
[2]*Departamento de Física Teórica and IFIC, Centro Mixto Universidad de Valencia-CSIC Institutos de Investigación de Paterna,*
Aptd. 22085, E-46071 Valencia, Spain
[3]*Departamento de Fisica, Universidad de los Andes, Cra.1E No. 18A-10, Santafe de Bogota, Colombia*

A study of the $pd \rightarrow pd\eta$ reaction in the energy range where the recent data from Uppsala are available is done in the two-step model of η production including the final state interaction. The $\eta-d$ final state interaction is incorporated through the solution of the Lippmann Schwinger equation using an elastic scattering matrix element, $T_{\eta d \rightarrow \eta d}$, which is required to be half off-shell. It is written in a factorized form, with an off-shell form factor multiplying an on-shell part given by an effective range expansion up to the fourth power in momentum. The parameters of this expansion have been taken from an existing recent relativistic Faddeev equation solution for the ηNN system corresponding to different $\eta-N$ scattering amplitudes. Calculations have also been done using few body equations within a finite rank approximation to generate $T_{\eta d \rightarrow \eta d}$. The $p-d$ final state interaction is included in the spirit of the Watson-Migdal prescription by multiplying the matrix element by the inverse of the Jost function. The $\eta-d$ interaction is found to be dominant in the region of small invariant $\eta-d$ mass, $M_{\eta d}$. The $p-d$ interaction enhances the cross section in the whole region of $M_{\eta d}$, but is larger for large $M_{\eta d}$. We find nearly isotropic angular distributions of the proton and the deuteron in the final state. All the above observations are in agreement with the data. The production mechanism for the entire range of the existing data on the $pd \rightarrow pd\eta$ reaction seems to be dominated by the two-step model of η production.

I. INTRODUCTION

The current great interest in the η-nucleus interaction exists because of the attractive nature of the $\eta-N$ interaction in the s wave [1] and the consequent possibility of the existence of quasibound, virtual, or resonant η-nucleus states [2]. The exact nature of these states, of course, depends upon the precise knowledge of the $\eta-N$ scattering matrix at low energies. As the η is a highly unstable meson (lifetime $\sim 10^{-18}$ s), this precise information is difficult to obtain directly. It can only be obtained from the η producing reactions through the final state interaction. With this motivation, starting with the early experiments near threshold at Saclay on the $pd \rightarrow {}^3$He η and the $pd \rightarrow pd\eta$ reactions, measurements have been carried out near threshold and beyond at Jülich and Uppsala using the COSY and Celsius rings, respectively. In this series of experiments, the recent data on the $pd \rightarrow pd\eta$ reaction using the Wasa/Promice setup at the Celsius storage ring of the Svedberg laboratory, Uppsala, are thematically complete and cover the excess energy, Q ($Q = \sqrt{s} - m_\eta - m_p - m_d$), ranging from around threshold to 107 MeV. The data [3] (integrated over other variables) include the invariant mass distribution over the whole excess energy range for the $\eta-d$, $\eta-p$, and $p-d$ systems and angular distributions for the proton, the deuteron, and the η meson. Like the $pd \rightarrow {}^3$He η reaction, the (inclusive)

$\eta-d$ invariant mass distribution exhibits a large enhancement near threshold and hence appears promising to study the $\eta-d$ interaction. The $\eta-p$ and $p-d$ invariant mass distributions do not show any such enhancement. All observed angular distributions are nearly isotropic.

Like in our earlier studies on the $pd \rightarrow {}^3$He η reaction, our primary aim in this article is to investigate the above-mentioned data on the $\eta-d$ invariant mass distribution to obtain a better understanding of the $\eta-N$ interaction as well as the $\eta-d$ interaction. We speculate, from our experience on the study of the $pd \rightarrow {}^3$He η reaction [4], that in the region of low $\eta-d$ relative energy this set of data will be mainly determined by the $\eta-d$ interaction, though the three-body nature of the final state may introduce some uncertainty in this conclusion.

We present a study of the $pd \rightarrow pd\eta$ reaction that includes the effect of the final state interaction. We have investigated two possible diagrams for the production mechanism: the direct mechanism and the two-step process of η production. The direct mechanism proceeds via an intermediate $pn \rightarrow d\eta$ reaction with one of the nucleons in the deuteron as a spectator. The η meson in the two-step model is produced in two steps, namely, $pp \rightarrow d\pi^+$ and $\pi^+N \rightarrow \eta N$, hence involving the participation and sharing of the transferred momentum by three nucleons. The two-step model for η production was first used in Ref. [5] and the data on the $pd \rightarrow {}^3$He η reaction was well explained. The vertices at the two steps have been described by the corresponding off-shell T matrices. The T matrix for $\pi^+N \rightarrow \eta N$ is taken from a coupled channel calculation [1] and that for $pp \rightarrow d\pi^+$ is obtained from the SAID program provided by the authors of Ref. [6].

―――――――
*Electronic address: neelam@physbu.mu.ac.in
†Electronic address: kanchan@ific.uv.es
‡Electronic address: brajeshk@gmail.com
§Electronic address: nkelkar@uniandes.edu.co

The final state interaction between the η and the deuteron is explicitly incorporated through an $\eta-d$ T-matrix, $T_{\eta d}$. This T matrix, which is required to be half-off-shell, is described in two ways. One choice involves taking a "factorized form," which is given by an off-shell form factor multiplied by an on-shell part given by an effective range expansion up to the fourth power in momentum. The parameters of this expansion have been taken from an existing recent relativistic Faddeev equation solution for the ηNN system [7] corresponding to different $\eta-N$ scattering amplitudes. The off-shell form factor is described in the following sections and is chosen to have a form without any adjustable parameters. The second prescription involves solving few body equations within the finite rank approximation (FRA) to obtain $T_{\eta d}$. This approach has been used in literature for the $\eta-d$, $-^3$He, and $-^4$He systems [8]. We perform calculations for both the prescriptions using different models of the elementary coupled channel η-nucleon T-matrix which characterize them.

The interaction between the η meson and the proton in the final state, to a certain extent, is contained implicitly in our calculations. This is due to the fact that we describe the $\pi^+ N \rightarrow \eta N$ vertex by a T matrix, which has been modeled to include the $\eta-N$ interaction. This off-shell T-matrix treats the πN, ηN, and $\pi \Delta$ channels in a coupled channel formalism [1] and reproduces the experimental data on this reaction very well.

The effect of $p-d$ final state interaction (FSI) is incorporated in the spirit of the Watson-Migdal FSI prescription [9], in which our model $pd \rightarrow pd\eta$ production amplitude is multiplied by a factor that incorporates the FSI between the proton and the deuteron. This factor is taken to be the frequently used [10–13] inverse Jost function, $[J(p)]^{-1}$, where p is the relative $p-d$ momentum. The assumption implicit in this approximation that the mechanism for the primary reaction be short ranged is very well fulfilled in the η-production reactions. The momentum transfer in these reactions near threshold is around 700 MeV/c. We include FSI for both doublet ($^2S_{1/2}$) and quadruplet ($^4S_{3/2}$) $p-d$ states.

The η-nucleon T-matrix, which characterizes our calculations, is not precisely known. Recent theoretical works on the $np \rightarrow d\eta$ reaction [14] conclude that the data on this reaction can be reproduced with the strength of the real part of the η-nucleon scattering length ranging between 0.42 and 0.72 fm. In our earlier work on the $pd \rightarrow {}^3$He η reaction [4], we found a good agreement with data, with the real part of the scattering length taken to be around 0.75 fm. This value was also found to be in agreement with the $np \rightarrow d\eta$ data in a K-matrix calculation of the final state $\eta-d$ interaction in Ref. [15]. The same authors as in Ref. [15] recently performed a fit to a wide variety of data that includes the $\pi N \rightarrow \pi N$, $\pi N \rightarrow \eta N$, $\gamma N \rightarrow \pi N$, and $\gamma N \rightarrow \eta N$ reactions and gave their best fit value of the η-nucleon scattering length, $a_{\eta N}$, to be $(0.91, 0.27)$ fm [16]. The $\eta-d$ effective range parameters are given in Ref. [7] for $a_{\eta N}$ up to $(1.07, 0.26)$ fm. Hence, in the present work we perform calculations with different models of the $\eta-N$ interaction, which correspond to three different values of the $\eta-N$ scattering length, ranging from $a_{\eta N} = (0.42, 0.34)$ fm to $(1.07, 0.26)$ fm.

We find that the cross sections calculated using the two-step model and the above inputs for the final state interaction reproduce most of the features of the experimental data reasonably well.

A theoretical effort to understand the Uppsala data [3] was made earlier by Tengblad, Fäldt, and Wilkin [17]. In Ref. [17] the contribution of three different diagrams, namely, the pickup (a direct one-step mechanism of η production), the impulse approximation, and the two-step mechanism (here the η meson is produced in two steps via the $pp \rightarrow \pi^+ d$ and $\pi^+ N \rightarrow \eta N$ reactions) to the cross section for the $pd \rightarrow pd\eta$ reaction is determined. The authors in Ref. [17] conclude that the impulse approximation is in general negligible as compared to the other two diagrams, the two-step mechanism is dominant in the near threshold region and the contribution of the pickup diagram (referred to as the direct mechanism in the present work) increases with energy and matches the two-step contribution at an excess energy of $Q = 95$ MeV. The latter conclusions regarding the contributions of the two-step and pickup diagrams are in contrast to the findings of the present work as well as to existing literature on similar kind of reactions. We note here that the authors in Ref. [17] do not include the final state interaction in their calculations in any way. They treat the kinematics and the dependence of the pion propagator (appearing in the two-step model) on the Fermi momenta in an approximate way. The T matrices that enter as an input to the two-step model are simply extracted from experimental cross sections and are hence not proper off-shell T-matrices. As a result of the above approximations, the authors in Ref. [17] do not reproduce the observed enhancement in the $\eta-d$ invariant mass distribution near threshold and, unlike the observed isotropic distributions, find anisotropy in their calculated angular distributions.

The contribution from the direct mechanism (or the so-called pickup diagram of Ref. [17]) to the total cross sections is found to be about four orders of magnitude smaller than the two-step contribution at threshold in the present work. The one-step contribution does increase with energy (as also found in Ref. [17]); however, even at the highest energy for which data are available ($T_p = 1096$ MeV), it remains two orders of magnitude smaller than that due to the two-step model. This is in contrast to the observations in Ref. [17], where the two processes give comparable contributions at high energies. The difference of orders of magnitude between the two processes can be understood as a result of the large momentum transfer, q, in the one-step process. This q, which is very large in the threshold region ($\sim$840 MeV/c), continues to be large even at high energies. For example, it is $\sim$600 MeV/c even at the highest beam energy of 1096 MeV. This finding of ours is very similar to the previous studies of the reactions involving high momentum transfer. For example, as mentioned above too, in Ref. [5], for the $pd \rightarrow {}^3$He η reaction up to 2.5 GeV beam energy, the authors comment that the one-step cross sections underestimate the data by more than two orders of magnitude. In yet another calculation [18] of the cross section for the $pd \rightarrow {}^3$HeX reaction (where $X = \eta, \eta', \omega, \phi$) the two-step model was found to describe the data on these reactions up to 3 GeV quite well. In Ref. [19], in connection with the $pd \rightarrow {}^3H_\Lambda K^+$ reaction, the authors claim that for a beam

energy of 1–3 GeV, the one-step mechanism predicts two to three orders of magnitude smaller cross sections as compared to the two-step mechanism. The cross sections obtained from the one-step model, in Ref. [17] are, however, reported to be only one order of magnitude less than those due to the two-step model at threshold and comparable to the two-step ones at high energies.

In the next section, we describe the details of the formalism. In the subsequent sections we present and discuss the results and finally the conclusions.

II. THE FORMALISM

The differential cross section for the $pd \rightarrow pd\eta$ reaction, in the center-of-mass, can be written as

$$d\sigma = \frac{m_p^2 m_d^2}{2(2\pi)^5 s |\vec{k}_p|} d\Omega_{p'} |\vec{k}_{p'}| dM_{\eta d} |\vec{k}_{\eta d}| d\Omega_{\eta d} \frac{1}{6} \langle |T|^2 \rangle, \quad (1)$$

where $\sqrt{s}$ is the total energy in the center-of-mass and $\vec{k}_p$ and $\vec{k}_{p'}$ are the proton momenta in the initial and final states, respectively. $M_{\eta d}$ denotes the invariant mass of the $\eta-d$ system and $\vec{k}_{\eta d}$ and $\Omega_{\eta d}$ denote, in the $\eta-d$ center-of-mass, the η momentum and its solid angle, respectively. $\Omega_{p'}$ represents the solid angle of the outgoing proton. Angular brackets around $|T|^2$ in Eq. (1) represent the sum over the final and initial spins.

The T matrix, which includes the interaction between the η and the deuteron, is given by

$$T = \langle \psi_{\eta d}(\vec{k}_{\eta d}), \vec{k}_{p'}; m_{p'}, m_{d'} | T_{pd \rightarrow pd\eta}$$
$$\times |\vec{k}_p, \vec{k}_d(= -\vec{k}_p); m_p, m_d \rangle, \quad (2)$$

where the spin projections for the proton and the deuteron in the initial and final states have been labeled as m_p, m_d, $m_{p'}$, and $m_{d'}$, respectively. $T_{pd \rightarrow pd\eta}$ is the production operator.

The wave function of the interacting $\eta-d$ in the final state is represented as $\psi_{\eta d}(\vec{k}_{\eta d})$. In terms of the elastic $\eta-d$ scattering T matrix, $T_{\eta d}$, it is written as

$$\langle \psi_{\eta d}^- | = \langle \vec{k}_{\eta d} | + \int \frac{d\vec{q}}{(2\pi)^3} \frac{\langle \vec{k}_{\eta d} | T_{\eta d} | \vec{q} \rangle}{E(k_{\eta d}) - E(q) + i\epsilon} \langle \vec{q} |. \quad (3)$$

The second term here represents the scattered wave. It has two parts originating from the principal value and the δ-function part of the propagator in the intermediate state. Physically they represent the off-shell and the on-shell scattering between the η and the deuteron. The on-shell part can be shown to be roughly proportional to the $\eta-d$ momentum and hence dominant at higher energies. The relative contribution of these terms in our case would be determined after we substitute the above expression for $\psi_{\eta d}(\vec{k}_{\eta d})$ in Eq. (2). We then get

$$T = \langle \vec{k}_{\eta d}, \vec{k}_{p'}; m_{p'}, m_{d'} | T_{pd \rightarrow pd\eta} | \vec{k}_p, \vec{k}_d(= -\vec{k}_p); m_p, m_d \rangle$$
$$+ \sum_{m_{2'}} \int \frac{d\vec{q}}{(2\pi)^3} \frac{\langle \vec{k}_{\eta d}; m_{d'} | T_{\eta d} | \vec{q}; m_{2'} \rangle}{E(k_{\eta d}) - E(q) + i\epsilon} \langle \vec{q}, \vec{k}_{p'}; m_{2'}, m_{p'} |$$
$$\times T_{pd \rightarrow pd\eta} | \vec{k}_p, \vec{k}_d; m_p, m_d \rangle. \quad (4)$$

It can be seen that the $T_{\eta d}$ here appears as a half-off-shell T-matrix.
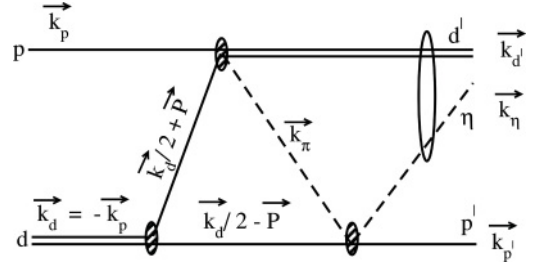

FIG. 1. The two-step process production mechanism for the $pd \rightarrow pd\eta$ reaction.

A. The production mechanism

For evaluating the η-production T-matrix, $\langle |T_{pd \rightarrow pd\eta}| \rangle$, we assume a two-step mechanism as shown in Fig. 1. In this model, the incident proton produces a pion in the first step on interacting with one of the nucleons of the target deuteron. In the second step this pion produces an η meson on interacting with the other nucleon. Both these nucleons are off-shell and have a momentum distribution given by the deuteron bound state wave function. To write the production matrix, we resort to certain standard approximations used in the literature [20] (in particular for the triangle diagram appearing in Fig. 1). The amplitude for the $pN \rightarrow \pi d$ process, which in principal is off-shell, is taken at an on-shell energy. Considering the high proton beam energy, off-shell effects are not expected to be significant. The $\pi N \rightarrow \eta N$ process is included via an off-shell T-matrix.

The production matrix is written as [4,5]

$$\langle |T_{pd \rightarrow pd\eta}| \rangle = \frac{3}{2} i \sum_{m's} \int \frac{d\vec{P}}{(2\pi)^3} \langle pn|d \rangle \langle |T_{pp \rightarrow \pi^+ d}| \rangle$$
$$\times \frac{1}{k_\pi^2 - m_\pi^2 + i\epsilon} \langle |T_{\pi^+ n \rightarrow \eta p}| \rangle, \quad (5)$$

where the squared four momentum of the intermediate pion, $k_\pi^2 = E_\pi^2 - \vec{k}_\pi^2$, with the energy E_π calculated at zero Fermi momentum and $\vec{k}_\pi = \vec{k}_\eta + \vec{k}_{p'} - \vec{k}_d/2 + \vec{P}$. The summation is over internal spin projections and the matrix element $\langle pn|d \rangle$ represents the deuteron wave function in momentum space, which has been written using the Paris parametrization [21]. The factor 3/2 is a result of summing the diagrams with an intermediate π^0 and π^+.

The integral over the pion momentum in the above includes the contribution from the pole as well as the principal value term. For the pion propagator itself, as can be seen, we have taken the plane wave propagator. This thus excludes any effect in our results due to medium modification of this propagator due to other nucleons. This aspect may be worth investigating in future.

The T matrix for the intermediate $pp \rightarrow \pi^+ d$ process has been taken from an energy-dependent partial wave analysis of the $\pi^+ d \rightarrow pp$ reaction from threshold to 500 MeV [6]. The various observables in Ref. [6] are given in terms of amplitudes that are parametrized to fit the existing database. We refer the reader to Ref. [6] and the references therein for the relevant expressions of the helicity and partial wave amplitudes and the notation followed by the authors in Ref. [6].
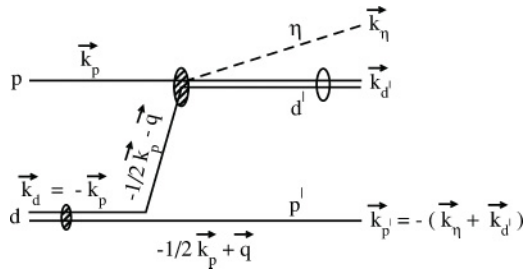
FIG. 2. The direct process production mechanism for the $pd \rightarrow pd\eta$ reaction.

For the $\pi^+ n \rightarrow \eta p$ subprocess, different forms of T matrices are available. We use the T matrix from Ref. [1] that treats the πN, ηN, and $\pi \Delta$ channels in a coupled channel formalism. This T matrix consists of the meson–N^* vertices and the N^* propagator as given below:

$$T_{\pi^+ n \rightarrow \eta p}(k', k; z) = \frac{g_{N^*}\beta^2}{(k'^2 + \beta^2)} \tau_{N^*}(z) \frac{g_{N^*}\beta^2}{(k^2 + \beta^2)}, \quad (6)$$

with

$$\tau_{N^*}(z) = (z - M_0 - \Sigma_\pi(z) - \Sigma_\eta(z) + i\epsilon)^{-1},$$

where $\Sigma_\alpha(z)$ ($\alpha = \pi, \eta$) are the self energies from the πN and ηN loops. The parameters of this model are $g_{N^*} = 0.616$, $\beta = 2.36$ fm^{-1}, and $M_0 = 1608.1$ MeV. This T matrix reproduces the data on the $\pi^+ n \rightarrow \eta p$ reaction very well.

Although the contribution of the direct mechanism (Fig. 2) is known to be small (owing to the large momentum transfer involved in the process) [5,18,19], for completeness, we calculate its contribution to the total cross section. The T matrix for this mechanism can be written as

$$\frac{1}{6}\langle |T_{pd \rightarrow pd\eta}|^2 \rangle = \frac{1}{4}\langle |T_{pn \rightarrow d\eta}(\sqrt{s_{\eta d}})|^2 \rangle \times |\phi_d(q)|^2, \quad (7)$$

where ϕ_d represents the deuteron wave function in the initial state. The spin summed $\langle |T_{pn \rightarrow d\eta}|^2 \rangle$ is given in terms of the total cross section for the $pn \rightarrow d\eta$ reaction by

$$\sigma_T(pn \rightarrow d\eta) = \frac{2m_p m_n m_d}{\pi s} \frac{|\vec{p}_f|}{|\vec{p}_i|} \frac{1}{4}\langle |T_{pn \rightarrow d\eta}|^2 \rangle, \quad (8)$$

where $\vec{p}_i$ and $\vec{p}_f$ are the initial and final momenta in the c.m. system. The momentum transfer $\vec{q}$, as shown in Fig. 2, is defined as

$$\vec{q} = \frac{1}{2}\vec{k}_p + \vec{k}_{p'}. \quad (9)$$

The total cross section, σ_T, for the $pn \rightarrow d\eta$ reaction is taken from the experiments [22].

B. Final state interaction

1. $\eta - d$ interaction

This is incorporated through a half-off-shell $\eta - d$ T-matrix. We construct this T matrix using the following two prescriptions.

a. Factorized form of $T_{\eta d}$. In one ansatz we obtain it by multiplying the on-shell $\eta - d$ T-matrix by an off-shell extrapolation factor $g(k', k)$. Requiring that this T matrix goes

to its on-shell value in the case of on-shell momenta, we write

$$T_{\eta - d}(k, E(k_0), k') = g(k, k_0)T_{\eta - d}(E(k_0))g(k', k_0), \quad (10)$$

with $g(p, q) \rightarrow 1$ as $p \rightarrow q$. For a half-off-shell case, this obviously is the ratio of the half-off-shell to the on-shell scattering amplitude.

For the on-shell $\eta - d$ T-matrix we use the effective range expansion of the scattering amplitude up to the fourth power in momentum,

$$F(k) = \left[\frac{1}{A} + \frac{1}{2}Rk^2 + Sk^4 - ik\right]^{-1}, \quad (11)$$

where F is related to T by

$$T_{\eta d}(k, k') = -\frac{1}{(2\pi)^2 \mu_{\eta d}} F_{\eta d}(k, E(k), k'). \quad (12)$$

The effective range expansion parameters (A, R, S) are taken from a recent relativistic Faddeev equation (RFE) calculation of Ref. [7]. This calculation uses the relativistic version of the Faddeev equations for a three-particle mNN system, where m is a meson and it can be an η, a π, or a σ meson. These particles interact pairwise, and these interactions are represented with separable potentials. The parameters of the $\eta N - \pi N - \sigma N$ potentials are fitted to the S_{11} resonant amplitude and the $\pi^- p \rightarrow \eta n$ cross sections. The $\eta - d$ effective range parameters obtained from these calculations are listed in Ref. [7] for different sets of the meson-nucleon potentials. Each of these sets gives a specific value of the $\eta - N$ scattering length, which is also listed in Ref. [7].

Because the half-off-shell extrapolation factor $g(k', k_0)$ is not known with any certainty, we choose the following two forms for it.

(i) Following the method in Ref. [15] for the final state interaction in the $\eta - d$ system, we express the off-shell form factor in terms of the deuteron form factor

$$g(k', k_0) = \int d\vec{r} j_0(rk'/2)\phi_d^2(r) j_0(rk_0/2), \quad (13)$$

where, for the deuteron wave function, $\phi_d(r)$, we take the Paris parametrization.

(ii) As a second choice, the form factor is taken to be the ratio of the off-shell $\eta - d$ T-matrix to its on-shell value, where both of them are calculated using the three body equations within FRA. The input to these calculations is the elementary $\eta - N$ scattering matrix, the details of which are given in the next section.

b. Few body equations within the finite rank approximation. The other prescription of $\eta - d$ FSI involves the use of the half-off-shell $\eta - d$ T-matrix obtained by solving few body equations within the finite rank approximation (FRA). For the details of this formalism and the expression for the η-nucleus T-matrix, we refer the reader to our earlier works [4]. To mention briefly, the FRA involves restricting the spectral decomposition of the nuclear Hamiltonian in the intermediate state to the ground state, neglecting thereby all excited and breakup channels of the nucleus. This is justified in the $\eta - {}^4$He and possibly in the $\eta - {}^3$He case,

but in η−deuteron collisions, where the breakup energy is just 2.225 MeV, the applicability of the FRA may be limited. However, it should be noted that a comparative study [23] of the η−d scattering lengths calculated using the FRA and the exact Alt-Grassberger-Sandhas (AGS) [24] equations (which include these intermediate excitations) shows that they are not very different if the real part of the η−N scattering length is restricted up to about 0.5 fm.

2. p−d interaction

We incorporate the p−d FSI in our calculations by multiplying our model T matrix by the inverse Jost function, $[J(p)]^{-1}$. We include the FSI in both the 1/2 and 3/2 spin states of p−d and restrict it to the s wave. Because the p and d are charged we also include the Coulomb effects. Following standard procedure, we write the Jost function in terms of phase shifts and use the effective range expansion for the later.

The complete expression for the s-wave inverse Jost function squared is written as

$$[J_o(k_{pd})]^{-2} = [J_o(k_{pd})]_Q^{-2} + \left[\left(1 + \frac{|E_B|}{E} \right) J_o(k_{pd}) \right]_D^{-2}. \quad (14)$$

Here, to include the effect of the existence of one bound state, namely, the spin 1/2 state (^{3}He), the doublet Jost function is multiplied by a factor $(1 + \frac{|E_B|}{E})$, where $|E_B|$ is the separation energy of ^{3}He into p−d. Its value is taken to be 5.48 MeV.

The expressions for spin quadruplet (Q) and doublet (D) $[J_o(k_{pd})]^{-2}$ are given by

$$[J_o(k_{pd})]_Q^{-2} = \frac{(k_{pd}^2 + \alpha^2)^2 (b_Q^c)^2}{4} \times \frac{1}{3C_o^2 k_{pd}^2} \left[\frac{2}{1 + \cot^2 \delta_Q} \right] \quad (15)$$

$$[J_o(k_{pd})]_D^{-2} = \frac{(k_{pd}^2 + \alpha^2)^2 (b_D^c)^2}{4} \times \frac{1}{3C_o^2 k_{pd}^2} \left[\frac{1}{1 + \cot^2 \delta_D} \right], \quad (16)$$

where

$$\alpha = \left(\frac{1}{b_\mu^c} \right) \left[1 + \left(1 + \frac{2b_\mu^c}{a_\mu^c} \right)^{\frac{1}{2}} \right], \quad (17)$$

and a_μ^c and b_μ^c are defined as

$$\frac{1}{a_\mu^c} = \frac{1}{C_o^2} \left[\frac{1}{a_\mu} - 2\gamma k_{pd} H_\gamma \right] \quad (18)$$

$$b_\mu^c = \frac{b_\mu}{C_o^2} \quad (19)$$

where μ stands for either Q or D. The factor C_o^2 in the above has its origin in the Coulomb interaction. The phase shifts $\delta_{Q,D}$ are obtained from an effective-range expansion [25,26],

$$C_o^2 k_{pd} \cot \delta_\mu = -\frac{1}{a_\mu} + \frac{1}{2} b_\mu k_{pd}^2 - 2\gamma k_{pd} H_\gamma \quad (20)$$

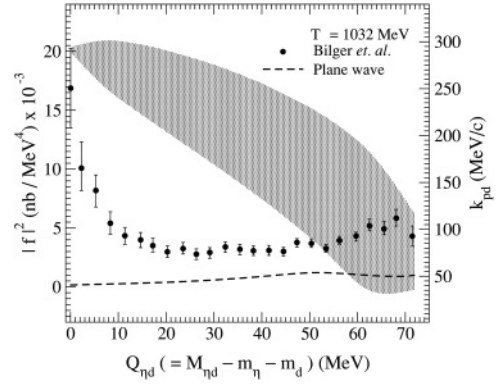$$\gamma = \frac{\alpha m_{\text{red}}}{\hbar k_{pd}} \quad (21)$$

FIG. 3. The ratio of experimental differential cross sections [3] to the phase space [Eq. (25)] as a function of the excess energy, $Q_{\eta d}$, along with range of p−d relative momenta, k_{pd} (hashed region), contributing to $|f|^2$ at each $Q_{\eta d}$.

$$C_o^2 = \frac{2\pi\gamma}{e^{2\pi\gamma} - 1} \quad (22)$$

$$H_\gamma = \sum_{n=1}^{\infty} \frac{\gamma^2}{n(n^2 + \gamma^2)} - \ln(\gamma) - 0.57722. \quad (23)$$

Here m_{red} is the reduced mass in the p−d system, γ is the Coulomb parameter, and α is the usual electromagnetic coupling constant. The values of the expansion coefficients a_μ, b_μ in Eq. (20) are taken as $a_Q = 11.88$ fm, $b_Q = 2.63$ fm, $a_D = 2.73$ fm, and $b_D = 2.27$ fm. They have been determined from a fit to the p−d elastic scattering phase shifts in the relative p−d momentum range up to around 200 MeV/c [27].

The above expression for the Jost function has the required property that, for large p, $J_0(p) \rightarrow 1$.

III. RESULTS AND DISCUSSION

Before we discuss the results of the present work, to highlight the FSI effects in the experimental η−d invariant mass distribution, we remove the phase space from the experimental $d\sigma/dM_{\eta d}$ and plot in Fig. 3 the $|f|^2$, which is then given by

$$|f|^2 = \frac{d\sigma}{dM_{\eta d}} \cdot \frac{1}{\text{phase space}}, \quad (24)$$

where

$$\text{phase space} = \frac{m_p^2 m_d^2}{12(2\pi)^5 s |\vec{k_p}|} \int d\Omega_{p'} |\vec{k_{p'}}| |\vec{k_{\eta d}}| d\Omega_{\eta d} \quad (25)$$

as a function of the excess energy, $Q_{\eta d} = M_{\eta d} - m_\eta - m_d$, where $M_{\eta d}$ is the invariant mass of the η−d system. In this figure we also show the plane wave result (i.e., $T_{pd \rightarrow pd\eta}$ does not include any FSI). The cross section, $d\sigma/dM_{\eta d}$ in Eq. (24), is evaluated for each $M_{\eta d}$ by performing an integral over the p−d center-of-mass momenta, k_{pd}. The range of the allowed values of k_{pd} at each $M_{\eta d}$ is shown by the hashed region. One clearly sees a large enhancement in the experimental $|f|^2$ near small values of $Q_{\eta d}$, which most likely is due to the η−d FSI. We also observe a rise at large values of $Q_{\eta d}$. Examining the
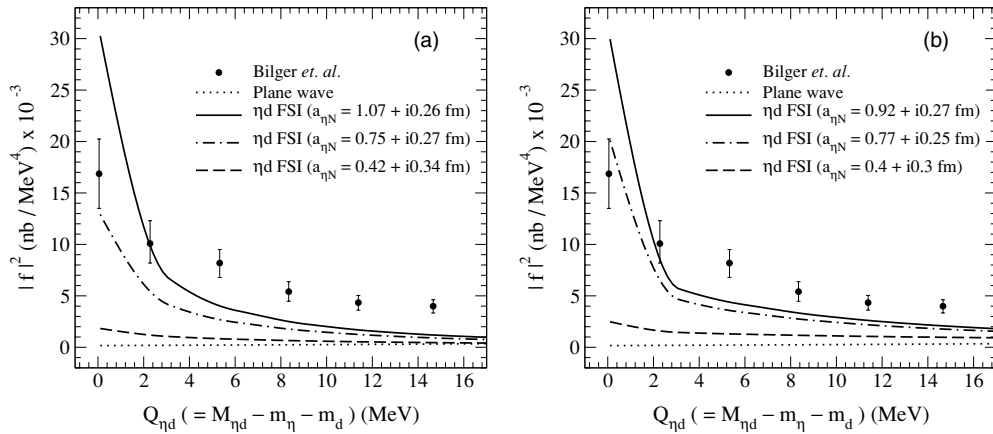
FIG. 4. The calculated $|f|^2$ along with the experimental results for a beam energy of 1032 MeV. (a) The results correspond to the factorized form of $T_{\eta d}$ with the off-shell factor generated from the deuteron form factor. (b) The results correspond to $T_{\eta d}$ obtained from few body equations within the FRA. The data are the same as in Fig. 3.

range of $p−d$ relative momenta that contribute to $|f|^2$ at each $Q_{\eta d}$, one can see that this rise occurs at small values of k_{pd}, indicating thereby the possibility of a large effect of $p−d$ FSI in this region.

In Fig. 4, we show two sets of the calculated $|f|^2$ along with the experimental results for a beam energy of 1032 MeV. These results include only $\eta−d$ FSI. We limit the range of $Q_{\eta d}$ up to about 10 MeV, where this effect is large. In Fig. 4(a) we show results for the factorized prescription with the off-shell factor generated from the deuteron form factor and the on-shell part arising from the relativistic Faddeev equation (RFE) calculation of Ref. [7]. The results are shown for three different sets of interaction parameters in the RFE. Because these sets give uniquely different values of the $\eta−N$ scattering lengths $a_{\eta N}$, we identify them by their corresponding $a_{\eta N}$ values. For the results presented here, these values are $0.42 + i0.34$ fm, $0.75 + i0.27$ fm, and $1.07 + i0.26$ fm. We see that our results reproduce the enhancement seen in the experimental $|f|^2$ at small values of $Q_{\eta d}$. The absolute magnitude depends upon the choice of the RFE parameters. It increases with $a_{\eta N}$, which designates these parameter sets.

The set corresponding to $a_{\eta N} = 1.07 + i0.26$ fm gives results closest to the experimental values.

In Fig. 4(b) we show $|f|^2$ calculated using few body equations within the FRA for $\eta−d$ FSI. These results are shown for three different inputs of the $\eta−N$ T-matrix taken from Ref. [16]. The choice of these T matrices is such that their scattering length values are close to those used in Fig. 4(a). Though this model has the limitation of retaining the intermediate nucleus in its ground state in the η-nucleus elastic scattering, the off-shell rescattering effects have been properly included. If we compare Figs. 4(a) and 4(b), the two sets of results are similar.

To check the sensitivity of the results to the off-shell form factor used in the factorized $\eta−d$ T-matrix, in Fig. 5(a), we show the $|f|^2$ calculated using two different off-shell form factors. The on-shell $T_{\eta d}$ is obtained from RFE and the off-shell part is either treated with a deuteron form factor (solid line) or a few body FRA form factor (dash dotted line) as explained in Sec. II B. The elementary $\eta−N$ T-matrix parameters required for the calculation of the FRA form factor are taken from the parametrization of Green and Wycech [16]. Even though the
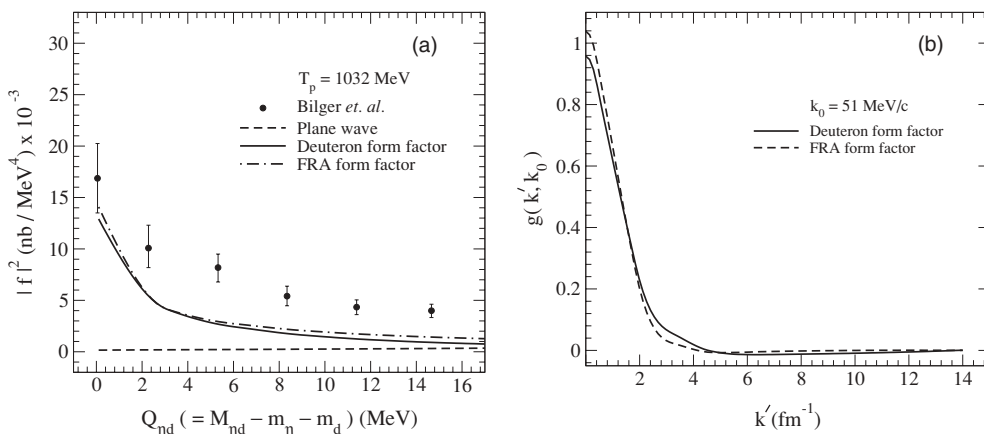

FIG. 5. Comparison of the two form factors for $a_{\eta N} = 0.75 + i0.27$ fm. (a) Effect of using two different off-shell extrapolation factors for $\eta−d$ FSI on $|f|^2$. (b) Two form factors as a function of off-shell momentum (k').

results [as shown in Fig. 4(a)] corresponding to the $a_{\eta N} = 1.07 + i0.26$ fm seem to be the closest to the data, to compare the effect of using different off-shell form factors, we choose the results corresponding to $a_{\eta N} = 0.75 + i0.27$ fm. We make this choice such that we can compare the two calculations for the inputs corresponding to a similar $\eta - N$ scattering length. It should be expected then that the off-shell form factors obtained from two different methods should not differ much. This is seen explicitly in Fig. 5(b) where the two form factors are shown as a function of off-shell momentum (k') for an on-shell value, k_0, near the low energy peak in the $\eta - d$ invariant mass distribution (to be discussed in Fig. 9 later).

Next, we include in our calculations the effect of the $p - d$ FSI. This is done by multiplying the $pd \to pd\eta$ squared T-matrix [Eq. (4)] used above by the inverse Jost function squared in Eqs. (15) and (16) and integrating it over the allowed range (as shown in Fig. 3) of $p - d$ momenta, k_{pd} for each $Q_{\eta d}$. We show these results in Fig. 6 for the RFE (with deuteron form factor) model of $\eta - d$ FSI, for the parameter set corresponding to $a_{\eta N} = 1.07 + i0.26$ fm. We find that the $p - d$ FSI affects the results in the whole region of $Q_{\eta d}$, while the effect of $\eta - d$ FSI is confined to small value of $Q_{\eta d}$. The large effect of $p - d$ FSI in the region of small $Q_{\eta d}$, however, may not be taken with confidence as the value of k_{pd} in this region is large (as shown in Fig. 3), where the s-wave effective range expansion [Eq. (20)] for the calculation of Jost function might not be sufficient. In any case, it appears that the effects of both the $\eta - d$ and the $p - d$ FSI on the $\eta - d$ invariant mass distribution are significant. If we disregard the calculated $p - d$ effect for small $Q_{\eta d}$, the $\eta - d$ and $p - d$ FSI dominate in regions well separated from each other.

Apart from the FSI, another important ingredient of our calculations is the two-step description of the production vertex. Because of the large momentum transfer, we believe, as has also been stressed in Ref. [17], that the angular distribution of the outgoing particles is probably more sensitive to the description of the production vertex. Inclusive angular distributions have been measured for all the three outgoing particles in the $pd \to pd\eta$ reaction. In Fig. 7, we show the calculated angular distributions for all the three outgoing particles along with the measured distributions. We show
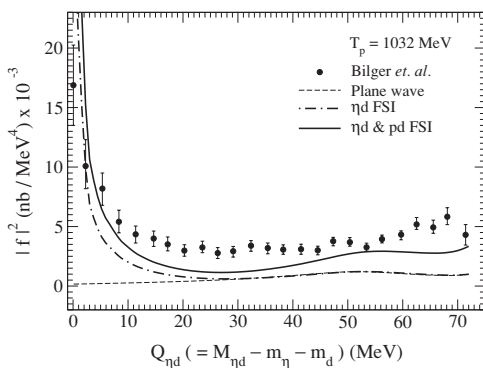

FIG. 6. The proton-deuteron final state interaction effects on the $pd \to pd\eta$ reaction at the beam energy of 1032 MeV. The dashed line shows the plane wave results and the dashed dot (solid) line shows the effect of $\eta - d$ ($\eta - d$ & $p - d$) FSI for $a_{\eta N} = 1.07 + i0.26$ fm.
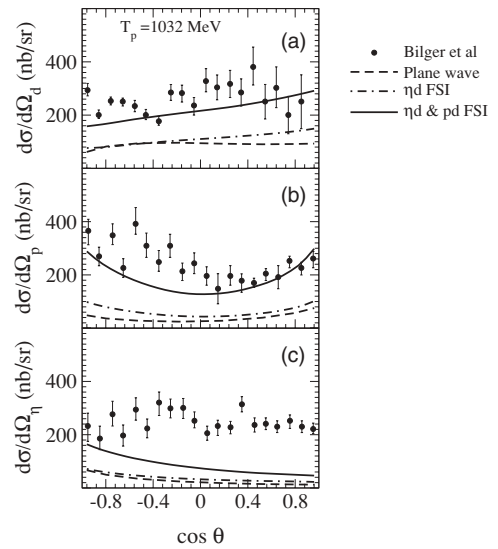

FIG. 7. The calculated angular distributions of (a) the deuteron, (b) the proton, and (c) the η, along with the measured cross sections for $a_{\eta N} = 1.07 + i0.26$ fm [3].

results without any FSI, with $\eta - d$ FSI and with both $\eta - d$ and $p - d$ FSI included. As each angle has a contribution from a range of $Q_{\eta d}$ as well as k_{pd}, the calculated results include integration of the cross section over these variables. We find that the observed nearly isotropic nature of the experimental angular distributions for the proton, deuteron, and η already gets reproduced by the plane wave calculations. The effect of both $\eta - d$ and $p - d$ FSI is large and persists over all the angles. Their inclusion brings the magnitudes of the proton and deuteron angular distributions near to experiments. The magnitude of the η distribution, however, does not seem to be affected much with the FSI.

Experimental data also exist on the total cross section. In Fig. 8, we compare the total cross sections calculated including both the $\eta - d$ and $p - d$ FSI with the measured cross sections.
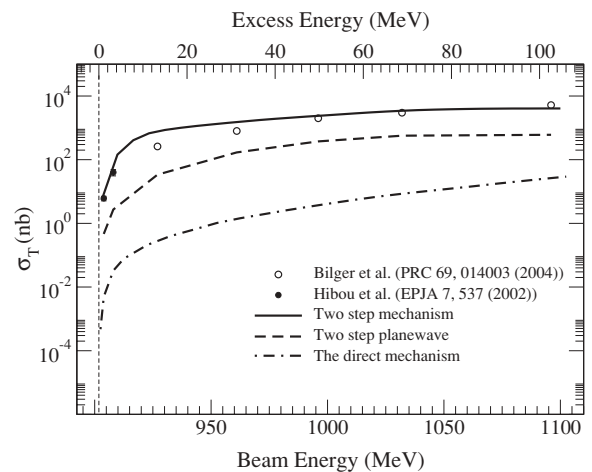

FIG. 8. A comparison of the total cross section for the $pd \to pd\eta$ reaction calculated with the description of the production vertex as a two-step mechanism and direct mechanism, along with the measured cross sections for $a_{\eta N} = 1.07 + i0.26$ fm [3,28].
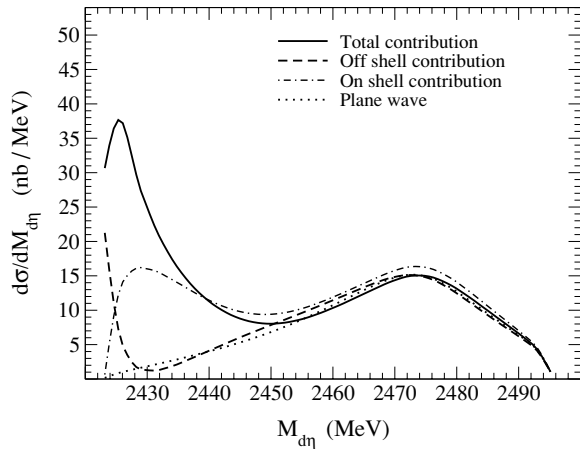
FIG. 9. Contributions from the off-shell and the on-shell $\eta-d$ scattering in the final state. The results are for $a_{\eta N} = 1.07 + i0.26$ fm with the inclusion of only the $\eta-d$ FSI.

FIG. 10. A comparison of the calculated results including both the $\eta-d$ and $p-d$ FSI with the experimental results. The results are for $a_{\eta N} = 1.07 + i0.26$ fm.

The results are shown with the factorized form of $\eta-d$ FSI with deuteron form factor for the set corresponding to $\eta-N$ scattering length equal to $1.07 + i0.26$ fm. As we see, the calculated cross sections are in good agreement with the experimental data.

In Fig. 8 we also give the cross sections calculated for the one-step direct mechanism (Fig. 2) mentioned in the previous section. Near threshold, these cross sections are about four orders of magnitude below those obtained from the two-step model and two orders of magnitude smaller in the high energy range. As mentioned in the Introduction, this observation is similar to that in other works involving large momentum transfer reactions [5,18,19] and is understandable because the momentum transfer continues to be large ($\sim$600 MeV/c) in the $pd \rightarrow pd\eta$ reaction even at an excess energy as large as 100 MeV.

Now we make an observation about the importance of off-shell scattering in treating $\eta-d$ FSI near threshold. The scattering part of the $\eta-d$ wave function [Eq. (3)] gets contributions from the off-shell as well as the on-shell scattering in the nucleus. To see quantitatively the relative importance of these two contributions to the cross section for the $pd \rightarrow pd\eta$ reaction, in Fig. 9 we show their contributions separately in the $\eta-d$ invariant mass distribution. These results include only the $\eta-d$ FSI generated from the factorized prescription using RFE and the deuteron form factor for the $\eta-d$ T-matrix. We find that near threshold the off-shell scattering completely dominates the threshold enhancement. At higher excess energy, as expected, the on-shell contribution takes over.

Finally we show the nature of agreement of our calculated results with the invariant $\eta-d$ mass distribution. In Fig. 10, we compare the calculated results including both the $\eta-d$ and $p-d$ FSI with the experimental results. The results are for $a_{\eta N} = 1.07 + i0.26$ fm calculated with the factorized prescription using RFE and the off-shell factor generated from the deuteron form factor. As we see the overall agreement is reasonably good.
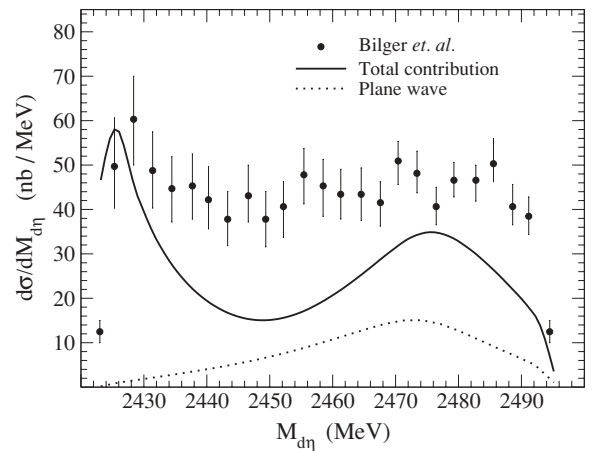
IV. SUMMARY

The invariant $\eta-d$ mass distribution in the $pd \rightarrow pd\eta$ reaction was studied by describing the production mechanism in terms of a two-step model with a pion being produced in the intermediate state. The $\eta-d$ FSI was included (a) in a factorized form involving an on-shell $T_{\eta d}$ and two types of off-shell form factors and (b) by solving few body equations within the FRA. The $p-d$ FSI was included through a Jost function. The conclusions of this investigation can be summarized as follows.

(i) Experimentally observed large enhancement in the cross section near small $\eta-d$ excess energy, $Q_{\eta d}$ is reproduced by the $\eta-d$ FSI. The rise in the cross section at large $Q_{\eta d}$ (which corresponds to a range of small proton and deuteron momenta, k_{pd}) can be accounted for by the $p-d$ FSI.

(ii) Quantitative reproduction of the large enhancement requires $\eta-d$ FSI corresponding to large values of $a_{\eta N}$. In the present calculation it is around $1.07 + i0.26$ fm.

(iii) The calculations successfully reproduce the observed isotropic angular distribution of the proton and the deuteron in the final state. The total cross sections for the $pd \rightarrow pd\eta$ reaction are also well reproduced.

(iv) The off-shell part of the $\eta-d$ scattering dominates near threshold.

(v) The results for two different choices of the off-shell extrapolation factor in the factorized form of the $\eta-d$ FSI are similar.

ACKNOWLEDGMENTS

[1] R. S. Bhalerao and L. C. Liu, Phys. Rev. Lett. **54**, 865 (1985).

[2] Q. Haider and L. C. Liu, Phys. Lett. **B172**, 257 (1986); **174**, 465(E) (1986); Phys. Rev. C **66**, 045208 (2002); N. G. Kelkar, K. P. Khemchandani, and B. K. Jain, J. Phys. G: Nucl. Part. Phys. **32**, L19 (2006); arXiv:nucl-th/0601080; for experimental claims, see M. Pfeiffer *et al.*, Phys. Rev. Lett. **92**, 252001 (2004) and references therein.

[3] R. Bilger *et al.*, Phys. Rev. C **69**, 014003 (2004).

[4] K. P. Khemchandani, N. G. Kelkar, and B. K. Jain, Nucl. Phys. **A708**, 312 (2002); Phys. Rev. C **68**, 064610 (2003).

[5] J. M. Laget and J. F. Lecolley, Phys. Rev. Lett. **61**, 2069 (1988).

[6] R. A. Arndt, I. I. Strakovsky, R. L. Workman, and D. V. Bugg, Phys. Rev. C **48**, 1926 (1993); The amplitudes can be obtained from the SAID program available at (http://gwdac.phys.gwu.edu).

[7] H. Garcilazo, Phys. Rev. C **71**, 048201 (2005).

[8] S. A. Sofianos and S. A. Rakityansky, in *Advances in Nuclear Physics* and Related Areas, Thessaloniki, 1997, edited by D. M. Brink, M. E. Grypeos, and S. E. Massen (Thessaloniki, Greece, Giahoudi-Giapouli Publishing, 1999), p. 570; arXiv:nucl-th/9707044; S. A. Rakityansky *et al.*, Phys. Rev. C **53**, R2043 (1996).

[9] K. M. Watson, Phys. Rev. **88**, 1163 (1952); A. B. Migdal, Zh. Eksp. Teor. Fiz. **28**, 3 (1955) [Sov. Phys.-JETP **1**, 2 (1955)].

[10] J. Gillespie, *Final State Interactions* (Holden-Day, San Francisco, 1964).

[11] M. L. Goldberger and K. M. Watson, *Collision Theory* (John Wiley & Sons, Inc., New York, 1964).

[12] R. Shyam, Phys. Rev. C **60**, 055213 (1999).

[13] J. Dubach, W. M. Kloet, and R. R. Silbar, Phys. Rev. C **33**, 373 (1986).

[14] H. Garcilazo and M. T. Peña, Phys. Rev. C **72**, 014003 (2005); **66**, 034606 (2002).

[15] S. Wycech and A. M. Green, Phys. Rev. C **64**, 045206 (2001).

[16] A. M. Green and S. Wycech, Phys. Rev. C **71**, 014001 (2005); see also the erratum in Phys. Rev. C **72**, 029902(E) (2005).

[17] U. Tengblad, G. Fäldt, and C. Wilkin, Eur. Phys. J. A **25**, 267 (2005).

[18] L. A. Kondratyuk and Yu. N. Uzikov, Yad. Fiz. **60**, 542 (1997) [Phys. At. Nucl. **60**, 468 (1997)]; arXiv:nucl-th/9510010.

[19] V. I. Komarov, A. V. Lado, and Yu. N. Uzikov, J. Phys. G: Nucl. Part. Phys. **21**, L69 (1995); arXiv:nucl-th/9804050; Yad. Fiz. **59**, 842 (1996) [Phys. At. Nucl. **59**, 804 (1996)].

[20] L. A. Kondratyuk and M. G. Sapozhnikov, Phys. Lett. **B220**, 333 (1989); L. A. Kondratyuk, A. V. Lado, and Yu. N. Uzikov, Yad. Fiz. **58**, 524 (1995) [Phys. At. Nucl. **58**, 473 (1995)]; A. Nakamura and L. Satta, Nucl. Phys. **A445**, 706 (1985); V. M. Kolybasov and N. Ya. Smorodinskaya, Phys. Lett. **B37**, 272 (1971).

[21] M. Lacombe *et al.*, Phys. Lett. **B101**, 139 (1981).

[22] H. Calèn *et al.*, Phys. Rev. Lett. **80**, 2069 (1998).

[23] N. V. Shevchenko, S. A. Rakityansky, S. A. Sofianos, V. B. Belyaev, and W. Sandhas, Phys. Rev. C **58**, R3055 (1998).

[24] E. O. Alt, P. Grassberger, and W. Sandhas, Nucl. Phys. **B2**, 167 (1967).

[25] H. A. Bethe, Phys. Rev. **76**, 38 (1949).

[26] H. O. Meyer and J. A. Niskanen, Phys. Rev. C **47**, 2474 (1993).

[27] J. Arvieux, Nucl. Phys. **A221**, 253 (1974).

[28] F. Hibou *et al.*, Eur. Phys. J. A **7**, 537 (2000).